05

Projected impact of climate change on the energy budget of the Arctic Ocean by a global climate model

James R. Miller
Dept.of Marine and Coastal Sciences
Cook College, Rutgers University
71 Dudley Road, New Brunswick, NJ 08901

Gary L. Russell
NASA/Goddard Space Flight Center
Institute for Space Studies, 2880 Broadway
New York, NY 10025

Submitted to Journal of Climate, October, 2001

Projected impact of climate change on the energy budget of the Arctic Ocean by a global climate model

James R. Miller
Gary L. Russell

Abstract

The annual energy budget of the Arctic Ocean is characterized by a net heat loss at the air-sea interface that is balanced by oceanic heat transport into the Arctic. The energy loss at the air-sea interface is due to the combined effects of radiative, sensible, and latent heat fluxes. The inflow of heat by the ocean can be divided into two components: the transport of water masses of different temperatures between the Arctic and the Atlantic and Pacific Oceans and the export of sea ice, primarily through Fram Strait. Two 150-year simulations (1950-2099) of a global climate model are used to examine how this balance might change if atmospheric greenhouse gases (GHGs) increase. One is a control simulation for the present climate with constant 1950 atmospheric composition, and the other is a transient experiment with observed GHGs from 1950 to 1990 and 0.5% annual compounded increases of CO_2 after 1990. For the present climate the model agrees well with observations of radiative fluxes at the top of the atmosphere, atmospheric advective energy transport into the Arctic, and surface air temperature. It also simulates the seasonal cycle and summer increase of cloud cover and the seasonal cycle of sea-ice cover. In addition, the changes in high-latitude surface air temperature and sea-ice cover in the GHG experiment are consistent with observed changes during the last 40 and 20 years, respectively.

Relative to the control, the last 50-year period of the GHG experiment indicates that even though the net annual incident solar radiation at the surface decreases by 4.6 Wm^{-2} (because of greater cloud cover and increased cloud optical depth), the absorbed solar radiation increases by 2.8 Wm^{-2} (because of less sea ice). Increased cloud cover and warmer air also cause increased downward thermal radiation at the surface so that the net radiation into the ocean increases by 5.0 Wm^{-2}. The annual increase in radiation into the ocean, however, is compensated by larger increases in sensible and latent heat fluxes out of the ocean. Although the net energy loss from the ocean surface increases by 0.8 Wm^{-2}, this is less than the interannual variability, and the increase may not indicate a long-term trend.

The seasonal cycle of heat fluxes is significantly enhanced. The downward surface heat flux increases in summer (maximum of 19 Wm^{-2} or 23% in June) while the upward heat flux increases in winter (maximum of 16 Wm^{-2} or 28% in November). The increased downward flux in summer is due to a combination of increases in absorbed solar and thermal radiation and smaller losses of sensible and latent heat. The increased heat loss in winter is due to increased sensible and latent heat fluxes, which in turn are due to reduced sea-ice cover. On the other hand, the seasonal cycle of surface air temperature is damped, as there is a large increase in winter temperature but little change in summer.

1. Introduction

The Arctic region is one of the key areas in trying to understand how climate might change in the future because it is where the powerful ice-albedo feedback mechanism operates. This feedback leads most global climate models to find enhanced warming in the Northern Hemisphere polar regions in transient studies with increasing atmospheric greenhouse gases (Houghton et al., 1996). Although there are some observational records to identify trends in parts of the Arctic Ocean, satellite data sets are only two decades old, and there is generally not enough long-term information to determine whether the trends are part of natural decadal variability or are the manifestation of climate change. Global climate models have the potential to address this question because they can simulate long-term trends. Serreze et al. (2000) address some of these issues in their summary of studies that document recent change in the northern high-latitude environment.

One of the earliest studies to quantify the various components (both radiative and turbulent) of the Arctic energy budget was that of Fletcher (1965). He used a combination of observations and results from other studies to compile energy budgets for the Arctic Basin at the surface and at the top of the atmosphere (TOA). Nakamura and Oort (1988) used a combination of satellites, rawinsondes, and models to calculate the atmospheric heat budget of both polar regions. Masuda (1990) confirmed their results for the north polar cap using an independent analysis based on data produced by the European Centre for Medium-Range Weather Forecasts (ECMWF). The availability of polar orbiting satellites during the last 20 years has helped in compiling better data sets of the Arctic radiative fluxes, both at the surface and at the TOA. However, there are still uncertainties in these fluxes, in part because of the nature of the observations themselves, and in part because of the algorithms used to convert satellite radiances into flux quantities. Chiacchio et al. (2001) and Key et al. (1996) have addressed some of these problems by comparing several different algorithms for the downward longwave flux at the surface in winter. More recently, there have been regional experiments to investigate the various components of the energy budget. One such experiment, the Surface Heat Budget of the Arctic Ocean (SHEBA), was conducted north of Alaska for a one year period between October, 1997 and October, 1998 (Andreas et al., 1999; Perovich et al., 1999; Curry et al., 2000).

There have been many studies of the Arctic region based on models ranging from one-dimensional column models through three-dimensional coupled atmosphere-ocean models. Tao et al. (1996) found that most of the three-dimensional atmospheric models had a 3 degree warm bias in the summer and that most of the models did a poor job of simulating the seasonal cycle of cloud cover. Both sea-surface temperature and sea-ice cover were prescribed in their study. Another recent inter-comparison study by Gates et al. (1999) compared the outputs of 31 different global models to prescribed surface conditions for a 10-year period. Rinke et al. (2000) compared two different regional climate models for the Arctic and found distinct differences between them. The Arctic is a region of great concern because of the feedbacks that exist and the potential impact of these feedbacks on global climate change. Unfortunately, the complexity of these feedbacks makes the region a difficult one to model, and the remoteness of the region has limited the observations. Randall et al. (1998) provide a good overview of the difficulties of modeling these complex interactions.

The purpose of this paper is to understand how the Arctic energy budget might change in the future in response to increases of atmospheric greenhouse gases and to understand the relationships among the different climate variables that might change. This is accomplished by using two 150-year simulations from the global climate model of Russell et al. (1995). The first simulation is a control with constant 1950 atmospheric composition, and the second is a GHG experiment with observed greenhouse gas concentrations from 1950 to 1990 and compounded 0.5% annual increases in CO_2 after 1990. These simulations are the same as those used by Miller and Russell (2000) to examine the Arctic freshwater budget. Russell et al. (2000) and Lucarini and Russell (2001) concluded that these model simulations faithfully represent actual climate changes during the past 40 years in the Northern Hemisphere. The climate model is described in the next section. The annual changes in the energy budget are given in Section 3, and the seasonal changes in Section 4. Section 5 contains a discussion and conclusions. An Appendix on model validation provides the reader with some insight on how well the model simulates the present climate.

2. The global climate model

The global synchronously coupled atmosphere-ocean model used in this study was developed by Russell et al. (1995) for climate studies at decade to century time scales. There are 9 vertical layers in the atmosphere and 13 in the ocean. The horizontal resolution for both the atmosphere and ocean is 4° in latitude by 5° in longitude. The resolution for heat, water vapor, and salt is finer than the grid resolution because those quantities have both means and directional gradients inside each grid cell. Atmospheric condensation and ocean vertical mixing are performed on $2^\circ \times 2.5^\circ$ horizontal resolution. The model has several new features including a new ground hydrology scheme, four thermodynamic layers for glacial ice and sea ice, advection of sea ice, glacial ice calving off Antarctica but not in the Northern Hemisphere, and the k-profile parameterization (KPP) ocean vertical mixing scheme of Large et al. (1994). Since the model does not use flux adjustments, there is some climate drift. To reduce its effect, predicted model changes are based on the subtraction of the control simulation from the transient GHG experiment.

Unlike rigid-lid ocean models, the present ocean model conserves mass and not volume, has a free surface, and does not use the Boussinesq approximation. The model conserves mass of salt globally at all times and uses natural boundary conditions for precipitation, evaporation, and river flow. The model transports mass, salt and heat through 12 sub-resolution straits including the Nares Strait on the west side of Greenland. Continental runoff and glacial ice melting eventually find their way back to the oceans via a river network based on Miller et al. (1994). For this study the area of the Arctic Ocean is 10^7 km^2 which is the same as that in Miller and Russell (2000). It does not include the Greenland-Iceland-Norwegian Sea nor Baffin Bay.

If the net mass crossing an interface by some process is zero, then the net energy transfer by that process can be measured without assuming anything about energy reference levels. If the net mass crossing an interface is not zero, then the energy transfer depends upon the assumed energy reference level, i.e. the zero reference temperature and the zero reference phase from which the

energy is measured. Hence, radiative transfer and sensible heating can be measured without requiring any assumptions about energy reference levels, but transport and evaporation do require it. The (zero) energy reference level for the atmosphere-ocean model is $0^{\circ}K$ for dry air and $0^{\circ}C$ for liquid water. Geopotential energy is measured from mean sea level. The energy content of water vapor contains its positive latent heat whereas the energy content of snow or sea ice is negative and is equal to the energy required to warm it to $0^{\circ}C$ and melt it to liquid water.

3. Changes in annual energy budget

In this section we examine changes in the annual energy budget of the Arctic Ocean between the GHG experiment and the control simulation. Since clouds and sea ice have a significant impact on the energy budget, their changes during the 150-year simulations are examined first. Figure 1 and Table 1 show that clouds are increasing in the GHG experiment, with the greatest changes in the last 50 years. Most clouds and most cloud changes are due to low clouds, defined in the model as those clouds between 740 mb and the surface. Although the model does allow clouds to form simultaneously at all levels, model diagnostics report only the highest clouds at each time step. Hence, low cloud amounts given in Table 1 are a lower bound because only the high cloud is counted when both high and low clouds are present. For the control simulation, the mean annual cloud cover varies between 60 and 65%.

Both cloud changes and sea-ice cover changes have important effects on the radiation budget of the Arctic Ocean. Figure 2 shows that sea-ice cover is decreasing in the GHG experiment. The model's rate of decrease is consistent with the observed rate of decrease in the Northern Hemisphere found by Parkinson et al. (1999) and Cavalieri et al. (1997) for the last two decades and with AMIP (see Fig. 2 for reference) for the last four decades of the 20^{th} century. Table 1 shows that there is also a significant decrease in sea-ice mass per unit area in the GHG experiment. Sea-ice mass can be converted to sea-ice thickness by dividing by the model's sea-ice density which is assumed to be 910 kg m^{-3}. Although there is some drift in the model's mean annual sea-ice cover for the present climate because it increases from 86% at the beginning to 88% at the end of the control simulation, the effect of the drift is mitigated by examining the differences between the GHG and control simulations. The model's annual export of sea-ice from the Arctic Ocean produces an energy import of 1.6 Wm^{-2} which decreases by 0.7 Wm^{-2} at the end of the GHG experiment.

The mean annual components of the energy budget are given in Table 2 with a positive sign denoting a downward vertical flux or an inward horizontal flux into the Arctic. The long-term changes in the radiative fluxes are shown in Fig. 3. Heating rate changes cited in this section are the difference between the last 50 years of the GHG experiment and the control simulation. At the top of the atmosphere (TOA) increased clouds cause greater atmospheric reflection, but that is more than compensated by less surface reflection because of reduced sea-ice cover. Thus, Fig. 3a shows that planetary albedo decreases, and planetary absorption of solar radiation increases by 3.2 Wm^{-2}. Increased low clouds, which are often warmer than the surface, cause greater thermal emission to space (Fig. 3b) by 1.4 Wm^{-2}, yet the change in net radiation at the TOA in the GHG

experiment (Fig. 3c) is still positive downward by 1.7 Wm^{-2}. This is slightly less than the model's global value of 1.8 Wm^{-2}.

Within the atmosphere, increased clouds cause atmospheric absorption of solar radiation to increase by 0.4 Wm^{-2} while thermal emission increases nine-fold to 3.7 Wm^{-2}. Increased clouds reduce atmospheric transmission, so that solar radiation incident on the surface (Fig. 4a) decreases by 4.6 Wm^{-2}. Nevertheless, Fig. 4b shows that solar radiation absorbed by the surface increases by 2.8 Wm^{-2} because of decreased sea-ice cover. Clouds and increased surface air temperature increase net thermal radiation into the surface (Fig. 4c) by 2.2 Wm^{-2} so that the total radiation there (Fig. 4d) increases by 5.0 Wm^{-2}. For the control simulation, there is no discernible drift in incident solar radiation at the surface (Fig. 4a), but there are downward drifts in both solar radiation absorbed by the surface (Fig. 4b) and net thermal radiation leaving the surface (Fig. 4c), consistent with the control's increasing sea-ice cover. For the GHG experiment, greater upward fluxes of sensible heat (2.9 Wm^{-2}) and latent heat (2.6 Wm^{-2}), and more snowfall (0.2 Wm^{-2}) are balanced by greater emission of radiation from the atmosphere (3.2 Wm^{-2}) and reduced atmospheric transport of heat into the Arctic air (2.5 Wm^{-2}).

These trends are significant for the radiation changes, for each individual component of the surface energy fluxes, and for sea-ice energy transport, whereas, for total surface heat flux and ocean heat transport, interannual variability exceeds the separation between the control and GHG simulations. Although both Fig. 5 and Table 2 show that the net loss of heat from the surface has increased for the last 50 years of the GHG experiment relative to the control, the opposite occurs in the period from 2000 to 2049. It is not clear from these simulations whether this is a trend or just natural variability. The results show that the advective heat loss due to reduced sea-ice export is nearly the same as the gain due to increased liquid heat import. Hence, there is little net change in total oceanic transport of heat into the Arctic Ocean. The interannual variability of ocean liquid heat transport is also high, and its change at the end of the GHG simulation shown in Table 1 might not represent a trend.

To summarize the mean-annual results, increased cloud cover and decreased sea-ice cover in the GHG experiment affect all components of the radiation and surface energy budgets. Greater cloud cover increases atmospheric reflection and absorption and decreases atmospheric transmission of solar radiation. Concurrently, atmospheric thermal emission, both upward and downward, increases. In spite of a decrease of solar radiation incident on the surface, absorption increases owing to reduced sea-ice cover. Net thermal radiation also increases into the surface. Reduced sea-ice cover causes turbulent fluxes to increase upward. Although the net upward summation of all surface fluxes increases marginally during the last 50 years of the GHG experiment, this may not be the result of climate change.

4. Changes in seasonal energy budget

Of perhaps greater interest than changes in the mean annual energy budget discussed in Section 3 are seasonal changes in the components of the energy budget. Seasonal changes in

polar regions are particularly striking because of the absence of solar radiation during winter. Tables 3 and 4 show the January and July changes for the various components of the energy budget over the Arctic Ocean. The heating rate changes cited in this section are for the last 50 years of the simulations and are shown in the last column of these tables.

As in Section 3, we first show how clouds and sea-ice cover change so that we can better understand how they affect the components of the energy budget. Clouds play a major role in reducing atmospheric transmission for both solar and thermal radiation. Fig. 6 shows that cloud cover increases significantly in winter in the GHG experiment, but there is little change in summer. The cloud optical depth increases in all months, but winter increases are larger. Figure 7 compares the monthly sea ice-cover for the control and GHG experiment. Sea ice covers less of the ocean in the GHG experiment during all months with the largest decrease (from 67% to 45%) occurring in September. In January the amount of open water doubles from 5% to 10%.

Changes in seasonal solar fluxes (Fig. 8) are similar to those in annual solar fluxes taking into consideration that incident solar radiation at the TOA varies from nearly zero in December to 505 Wm^{-2} in June. Figure 8 shows that the absorbed solar radiation at the TOA increases in all months in the GHG experiment. Even though the incident solar radiation at the sea surface decreases in all months (not shown), the absorbed solar radiation at the surface increases in all months. The changes in the seasonal cycles of both sea-ice cover (greater reduction in summer) and clouds (more in winter) enhance the absorption of solar radiation at the TOA and at the surface, more than if sea-ice and cloud changes were distributed uniformly throughout the year.

Changes in seasonal thermal fluxes (Fig. 9) require explanations. In winter, the cloud layer is warmer than both the surface and the upper atmosphere. Because there are more clouds, atmospheric thermal emission increases (6.4 Wm^{-2}) sending its radiation both upward and downward. Outgoing thermal radiation at the TOA increases by 3.2 Wm^{-2}. Upward thermal radiation at the surface increases for two reasons in winter: there is more open water whose ocean temperature is considerably warmer than that of sea-ice and the surface temperature of sea ice is warmer in the GHG experiment. Nevertheless, downward thermal radiation still dominates at the surface and the net upward emission decreases by 3.2 Wm^{-2}. In summer, the temperature contrast between ocean and ice disappears and the surface is warmer than the cloud layer. The small increase in cloud optical thickness further insulates the warm surface from outer space while hardly changing the net atmospheric thermal emission. Upward thermal radiation decreases by 1.0 Wm^{-2} at the TOA and by 0.9 Wm^{-2} at the surface in summer.

The changes in atmospheric energy transport into the Arctic in the GHG experiment are different between winter and summer (Tables 3-4). The transport is reduced in winter, in part because the significantly higher polar surface air temperature weakens the wintertime pole to equator temperature gradient. The transport is higher in summer because the gradient is stronger. Although the atmospheric transports in the Arctic respond to changes in other processes, it is also likely that they participate in driving some of the Arctic changes.

Figure 10 shows the net heating at the surface. During winter, the net heat loss out of the

Arctic Ocean increases by 10 to 16 Wm^{-2}, and during summer the flux into the ocean increases by almost 20 Wm^{-2} in June. As noted in section 3 (Fig. 5 and Table 2), the variability in mean annual net heating of the ocean surface between the three different 50-year periods of the GHG experiment makes it difficult to determine whether there is a long-term trend. This is in contrast to the unambiguous seasonal changes in net surface heating where the seasonal cycle is significantly enhanced. The reduction of upward surface heat flux by radiation, in January (Table 3), is overwhelmed by increases of the other components (8.4 Wm^{-2} by sensible heat, 5.2 Wm^{-2} by latent heat, 0.7 Wm^{-2} by precipitation heat). The turbulent fluxes in winter are proportional to the open water fraction; both the fluxes and open water nearly double in January. In July (Table 4), the warmer, moister Arctic air reduces the effectiveness of the turbulent fluxes, and their small changes are now additive to the increased solar absorption.

Figure 11 shows that the ocean liquid heat transport into the Arctic Ocean increases in all months in the GHG experiment with the largest increases (15%) occurring in July, November and December. However, there is no significant change in total ocean heat transport because the increase in liquid transport is opposed by a decrease in sea-ice heat transport. Table 3 shows that the changes are almost exactly offsetting in January but that the change in liquid transport is higher in summer. The other component of the water transport is due to river flow. Tables 3 and 4 show that the changes in heat transport due to river flow are small in both January and July.

The seasonal results can be summarized as follows. Cloud cover (except in summer) and cloud optical depth increase while sea-ice cover decreases in all seasons. The reduced sea-ice cover causes absorbed solar radiation into the ocean to increase in summer and upward turbulent fluxes to increase in winter, both of which enhance the seasonal cycle of surface energy fluxes. In winter, when the cloud layer is warmer than the temperature above and below it, increased cloud cover causes thermal radiation to enhance the radiative seasonal cycle at the TOA but to reduce the enhancement of upward surface fluxes which are dominated by the turbulent fluxes. In summer, greater cloud optical thickness insulates the surface from space. This reduces net upward thermal radiation whose change is now additive to the increased solar radiation which dominates. The warmer, moister surface air also reduces the upward turbulent fluxes. Thus, each term of the TOA and surface fluxes enhances the seasonal cycle in summer. The ultimate fate of the annual surface energy budget will depend upon which of the seasonal trends is larger. This depends on the magnitude of the trends and on the number of months during which they occur. It presently appears that the winter trends are smaller, but extend over more months.

5. Discussion and conclusions

The simulations in this paper are the same as those used to examine potential changes in the Arctic freshwater and mass budgets (Miller and Russell, 2000). In the GHG experiment there are net increases of river flow, precipitation, and evaporation and net decreases of sea-ice cover and sea-ice export from the Arctic Ocean. As shown here, the net decrease in sea-ice export leads to a net reduction in total oceanic heat flux into the Arctic Ocean because the heat content of sea ice is negative.

The mean annual results and seasonal results are summarized in the last paragraphs of Sections 3 and 4. Changes in the mean annual components of the energy budget and related variables are the sum of seasonal changes that are often quite different, and in some cases, of opposite sign. The amplitudes of the seasonal cycles of the following variables increase in the GHG experiment: sea-ice cover, solar radiation absorbed at TOA and surface, net radiation at TOA, turbulent heat fluxes, and net heating at the surface. Other variables whose amplitudes decrease include cloud cover, atmospheric poleward heat transport, and surface-air temperature. When the mean annual change is the difference between large seasonal changes of the same magnitude, but opposite sign, it may be difficult to determine the mean annual change. An example of this is the net heating at the surface for which there is a significant increase of heat into the ocean in summer and out of the ocean in winter. The GHG experiment, however, does not allow one to conclusively determine whether there is a net change or trend in the mean annual surface heating.

Changes in surface air temperature are closely related to changes in the energy budget. Table 1 shows that the mean annual surface air temperature increases by 3.4° C during the last 50-year period of the GHG experiment, and Fig. 12 shows that it increases in all months. It does not, however increase uniformly in all months. The increases are up to 6 degrees in winter, smaller in spring and autumn, and quite small in summer. Although the changes in surface air temperature occur in response to changes in local heating and larger scale changes in atmospheric circulation, much of the increase in the GHG experiment can be explained by local processes. The increased amplitude of the annual cycle of net surface heating is consistent with the reduced amplitude for surface air temperature. The increased heat flux from the ocean in winter increases the surface air temperature significantly while the increased heat flux into the ocean in summer has little effect on the summer air temperature.

Serreze et al. (2000) indicate that most climate models find the greatest Arctic warming in autumn and winter, but observations show greater warming from winter through early summer, presumably because of increased atmospheric heat flux into the region. The atmospheric heat transport into the Arctic does increase in summer in the GHG experiment, but it does not cause much change in the surface air temperature, which is constrained by the presence of sea ice and surface ocean temperatures that can not increase much above the freezing point. The model indicates that the large increases in winter are primarily due to local processes. In fact, the model's decreased atmospheric heat transport into the Arctic in winter tends to reduce the warming. Serreze et al. (2000) are careful to point out that change in the Arctic is still difficult to observe for many reasons. There are few data in many regions, the changes that have occurred during the last 40 years occur in part because of changes in the North Atlantic Oscillation (NAO), and some of the data are difficult to interpret.

The changes in the model's surface air temperature in the GHG experiment are discussed in greater detail in Russell et al. (2000) and in Lucarini and Russell (2001). They showed that the model's surface air temperature and pressure changes during the last 40 years are well correlated with observed changes in the Northern Hemisphere winter. The model does show an increase in the NAO index during this period, but its magnitude is smaller than the observed increase.

There are many complex interactions among radiation, clouds, and the surface in the Arctic Ocean. Although some of these interactions have been discussed in this paper, there are many others that are considered in a comprehensive treatment by Fletcher (1965). He notes that solar radiation reflected upward from the surface in summer is reflected back downward by clouds; the diffuse component of solar radiation is often significantly higher than the direct component; and the melt of snow and ice and the subsequent puddling of liquid water on sea ice can significantly alter the surface albedo in summer. The model does account for downward reflection of sunlight by cloud and does distinguish between direct and diffuse radiation, but we have not quantified these effects. The model, however, does not include puddling, which means that the model's surface albedo is likely to be somewhat too high in the summer. In the model, the surface albedo of sea-ice decreases to 45% after the snow has melted. A portion of the model's lower than observed surface-air temperature in summer could be caused by a surface albedo that is too high.

It is difficult to sort out all the related feedbacks that interact to produce the changes in the components of the energy budgets in the GHG experiment. For sea-ice alone there are seasonally varying changes in albedo, thickness, and geographic coverage. For clouds there are seasonally varying changes in total cloud cover, high and low clouds, and optical depth. In addition, there is an increase in atmospheric water vapor with the largest increase occurring in summer. Changes in these variables affect the surface radiative and turbulent fluxes. One example of the competing interactions between sea ice and clouds is the increase in absorbed solar radiation at the TOA and surface in the GHG experiment. At the TOA the absorbed solar radiation increases in spite of the increased reflectivity of the atmosphere (more clouds). At the surface reduced sea-ice cover accounts for the absorbed solar radiation increasing in spite of a decrease in incident solar radiation.

Rind et al. (1995, 1997) used a very different model to determine how the sea-ice albedo feedback mechanism interacts with other feedbacks, particularly those related to clouds and water vapor. They found that the total effect of sea ice, including feedbacks, accounted for about one third of the global change in surface air temperature in a doubled CO_2 simulation. They also found that the effect was four times larger than an analysis that left out cloud and water vapor feedbacks that resulted from changes in sea-ice cover. The GHG results here are consistent with their results in winter when the largest increase in surface air temperature occurs, in part, because increased clouds and water vapor enhance the surface warming in winter.

We believe that the internal self-consistency of the model and the ability to compare the results here with the changes in the hydrologic cycle discussed in Miller and Russell (2000) help to frame some of the questions related to potential climate change in the Arctic region. In light of the many difficulties in both observing and modeling the Arctic region, we hope that other climate modelers will focus on potential changes in the Arctic energy budget to determine whether their results are similar to or significantly different from those presented here. The results in this paper are for the entire Arctic Ocean. We have not examined spatial variability within the Arctic, but the changes identified in this paper are generally more pronounced at sea-ice boundaries and in the Barents Sea.

APPENDIX: Validation of Control Simulation for Present Climate

Reliable observations of most geophysical quantities in the Arctic are lacking so model validation is difficult. In this section we provide information about the model's control simulation to provide some indication of how well the model represents the various components of the energy budget. Of all the components of the Arctic energy budget, those for which we have the most reliable observations are the TOA radiative fluxes. Figures 8 and 9 show that the model is in generally good agreement with the satellite observations from ERBE. Our results can be compared with those of Nakamura and Oort (1988) who use a combination of satellites, rawinsondes, and models to compile an Arctic energy budget and with the analysis of Masuda (1990). The comparison is not exact because our study is for the Arctic Ocean and theirs was for the latitude band between 70 and 90 north. The absorbed solar radiation at the TOA in our study is maximum in summer at 235 Wm^{-2} compared to Nakamura and Oort's 210 Wm^{-2}.

Based on Table 2 the control simulation's net annual radiation into the Arctic Ocean is 13.6 W m^{-2}. The results for the net annual radiative fluxes at the surface are within 10 Wm^{-2} of the observations of Nakamura and Oort (1988). The surface radiative fluxes are difficult to observe, particularly thermal radiation. Beesley et al. (2000) indicate that there can be model errors of 10 Wm^{-2} in the downward thermal radiation in winter when low clouds are present. Chiacchio et al. (2001) and Key et al. (1996) compare several different methods for retrieving downward thermal fluxes in winter and find biases ranging from –34 Wm^{-2} to nearly zero. Chiacchio et al. (2001) conclude that the possible sources of errors include clouds that are too thin, lack of cloud overlap techniques, incomplete parameterizations, and inconsistencies between surface and satellite measurements. Schweiger and Key (1994) find errors up to 20 Wm^{-2} between different observations of net surface radiation.

Many global climate models do a poor job of representing the seasonal cycle of cloud cover in the Arctic Ocean (Tao et al., 1996). The model used here does successfully capture the seasonal cycle of cloud cover as shown in Fig. 6. For the control, the cloud optical depth varies between 3 in winter and 13 in summer. Using observations of Arctic clouds, Kukla and Robinson (1988) found a range of 2 to 25 for optical depth, and Curry and Ebert (1992) obtained values between 2 and 8 when weighted by cloud fraction.

Beesley and Moritz (1999) addressed the interesting question of why the Arctic cloud cover increases in summer. They used a radiative-turbulent column model to investigate three hypotheses: 1) advection from the land mass of air masses of higher specific humidity than over the pack ice, 2) evaporation at the surface of the pack ice, and 3) a temperature dependent formation and precipitation of atmospheric ice. Their model suggests that the third hypothesis is important in the increase in summertime cloudiness. An observational study by Kukla and Robinson (1988) tends to support the first hypothesis. Our model allows us to comment on the first two hypotheses, and although the third process is included, too, we cannot easily identify its effects. For the control simulation, 44% of the precipitation is derived from local evaporation and 56% is derived from atmospheric moisture advection into the Arctic. For the GHG experiment, this shifts to about 50% for each.

Table 2 shows that the net heat into the surface in the control is -10.35 Wm^{-2} (i.e., away from the surface). The upward sensible and latent heat fluxes are of comparable magnitude (11.5 and 9.8 Wm^{-2}) and the energy of precipitation (snow) is 2.7 Wm^{-2}. The control run is not in balance as indicated by the net energy change (0.44 Wm^{-2}) in Table 2. The model's mean annual atmospheric heat transport into the Arctic region (103 Wm^{-2}) is also consistent with Nakamura and Oort's 98 Wm^{-2} and with the value of 102 Wm^{-2} found by Masuda (1990). As shown in Table 2, the model's oceanic heat transport for the present climate is 10.7 Wm^{-2} (9.1 ocean liquid transport and 1.6 sea-ice transport) which is in good agreement with the observations of Aagaard and Greisman (1975). The model's seasonal cycle of sea-ice cover indicates that there is too much sea ice in all months in comparison with the AMIP observations (Fig. 7). The model's seasonal cycle of surface air temperature is in good agreement with observations (Fig. 12) although somewhat too low in summer.

Acknowledgments. Partial support for JRM has been provided under Project #32103 of the New Jersey Agricultural Experiment Station. We are grateful to Jennifer Francis for reviewing and providing helpful suggestions on the manuscript. Additional information about these simulations is available at http://aom.giss.nasa.gov.

References:

Aagaard K, and P. Greisman, 1975: Toward new mass and heat budgets for the Arctic Ocean. J. Geophys. Res., 80, 3821-3827.

Andreas, E.L., C.W. Fairall, P.S. Guest, and P.O.G. Persson, 1999: An overview of the SHEBA atmospheric surface flux program. Paper presented at 5th Conference on Polar Meteorology and Oceanography, Am. Meteorol. Soc., Dallas, TX, Jan. 10-15, 1999.

Beesley, J.A., 2000: Estimating the effect of clouds on the arctic surface energy budget. J. Geophys. Res., 105, 10,103-10,117.

Beesley, J.A., and R.E. Moritz, 1999: Toward an explanation of the annual cycle of cloudiness over the Arctic Ocean. J. Climate, 12, 395-415.

Cavalieri, D.J., C.L. Parkinson, P. Gloersen, and H.J. Zwally, 1997: Arctic and Antarctic sea ice concentrations from multichannel passive microwave satellite data sets: October 1978 to September 1995, user's guide, NASA Tech. Memo., TM-104627, 17pp.

Chiacchio, M., J. Francis, and P. Stackhouse, 2001: Evaluation of methods to estimate the surface downwelling longwave flux during Arctic winter. J. Appl. Meteor., in press.

Curry, J.A., and E.E. Ebert, 1992: Annual cycle of radiation fluxes over the Arctic Ocean: Sensitivity to cloud optical properties. J. Climate, 5, 1267-1280.

Curry, J.A., and 26 others, 2000: FIRE Arctic Clouds Experiment. Bull. Amer. Meteorol. Soc., 81, 5-29.

Fletcher, J.O., 1965: The heat budget of the Arctic Basin and its relation to climate. The Rand Corp., 175 pp.

Gates, W.L., and 15 others, 1999: An overview of the results of the atmospheric model intercomparison project (AMIP). Bull. Amer. Meteor. Soc., 80, 29-55.

Houghton, J.T., L.G. Meira Filho, B.A. Callander, N. Harris, A. Kattenberg, and K. Maskell, (Eds.), 1996: Climate Change 1995: The Science of Climate Change. Cambridge Univ. Press, 572 pp.

Huschke, R., 1969: Arctic cloud statistics from "air-calibrated" surface weather observations. The Rand Corp., 79 pp.

Key, J., R.S. Silcox, and R.S. Stone, 1996: Evaluation of surface radiative flux parameterizations for use in sea ice models. J. Geophys. Res., 101 (C2), 3839-49.

Kukla, G.J., and D.A. Robinson, 1988: Variability of summer cloudiness in the Arctic Basin. Meteorol. Atmos. Phys., 39, 42-50.

Large, W.G., J.C. McWilliams, and S.C. Doney, 1994: Oceanic vertical mixing: Review and a model with non-local boundary layer parameterization. Rev. Geophysics, 32, 363-403.

Lucarini, V., and G.L. Russell, 2001: Comparison of mean climate trends in the northern hemisphere between N.C.E.P. and two atmosphere-ocean model forced runs. Submitted to J. Geophys. Res. (Atmos.).

Masuda, K., 1990: Atmospheric heat and water budgets of polar regions: Analysis of FGGE data. In Proc. of the Nat. Inst. Polar Res. Symp. On Polar Meteorol. And Glaciol., Tokyo, 3, Jan. 1990, 79-88.

Miller, J.R., and G.L. Russell, 2000: Projected impacted of climate change on the freshwater and salt budgets of the Arctic Ocean by a global climate model. J. Geophys. Res., 27, 1183-1186.

Miller, J.R., G.L. Russell, and G. Caliri, 1994: Continental scale river flow in climate models. J. Clim., 7, 914-928.

Nakamura, N., and A.H. Oort, 1988: Atmospheric heat budgets of the polar regions. J. Geophys. Res., 93, 9510-9524.

Parkinson, C.L., D.J. Cavalieri, P. Gloersen, H. J. Zwally, and J.C. Comiso, 1999: Arctic sea ice extents, area, and trends, 1978-1996. J. Geophys. Res., 104, 20,837-20,856.

Peixoto, J.P., and A.H. Oort, 1992: Physics of Climate. American Inst. Physics, 520 pp.

Perovich, D.K., and 22 others, 1999: Year on ice gives climate insights. EOS, 80, 481.

Randall, D., J. Curry, D. Battisti, G. Flato, R. Grumbine, S. Hakkinen, D. Martinson, R. Preller, J. Walsh, and J. Weatherly, 1998: Status of and outlook for large-scale modeling of atmosphere-ice-ocean interactions in the Arctic. Bull. Amer. Meteor. Soc., 79, 197-219.

Rind, D., R. Healy, C. Parkinson, and D. Martinson, 1995: The role of sea ice in 2 x CO2 climate model sensitivity. Part I: The total influence of sea-ice thickness and extent. J. Climate, 8, 449-463.

Rind, D., R. Healy, C. Parkinson, and D. Martinson, 1997: The role of sea ice in 2xCO2 climate model sensitivity: Part II: Hemispheric dependencies. Geophys. Res. Let., 24, 1491-1494.

Rinke, A., A.H. Lynch, and K. Dethloff, 2000: Intercomparison of Arctic regional climate simulations: Case studies of January and June 1990. J. Geophys. Res., 105, 29,669-29,683.

Russell, G.L., J.R. Miller, and D. Rind, 1995: A coupled atmosphere-ocean model for transient climate change studies. Atmos.-Ocean, 33, 683-730.

Russell, G.L., J.R. Miller, D. Rind, R.A. Ruedy, G.A. Schmidt, and S. Sheth, 2000: Comparison of model and observed regional temperature changes during the past 40 years. J. Geophys. Res., 105, 14,891-14,898.

Schweiger, A.J., and J.R. Key, 1994: Arctic ocean radiation fluxes and cloud forcing based on the ISCCP-C2 cloud dataset. J. Appl. Meteor., 33, 948-963.

Serreze, M.C., J.E. Walsh, F.S. Chapin III, T. Osterkamp, M. Dyurgerov, V. Romanovsky, W.C. Oechel, J. Morison, T. Zhang, and R.G. Barry, 2000: Observational evidence of recent change in the northern high-latitude environment, Clim. Change, 46, 159-207.

Shea, D., 1986: Climatological atlas, 1950-1979: Surface air temperature, precipitation, sea-level pressure and sea-surface temperature (45°S-90°N), Tech. Note/TN-269+STR, Nat. Cent. For Atmos. Res., Boulder, CO.

Tao, X., J.E. Walsh, and W.L. Chapman, 1996: An assessment of global climate simulations of Arctic air temperatures. J. Clim., 9, 1060-1076.

Figure Captions.

Figure 1. Mean annual cloud cover for Arctic Ocean for control and GHG experiment.
Figure 2. Sea-ice cover for control and GHG experiment. For the observations GSFC (Goddard Space Flight Center) is from Cavalieri et al. (1997) and the AMIP values can be downloaded from http://www-pcmdi.llnl.gov/amip2/AMIP2EXPDSN/BCS/amipobs_dwnld.html.
Figure 3. Top of the atmosphere radiation budget for Arctic Ocean for control and GHG experiment for (a) absorbed solar, (b) outgoing thermal, and (c) net downward radiation.
Figure 4. Modeled downward radiation at surface of Arctic Ocean for control and GHG experiment for (a) incident solar radiation, (b) absorbed solar radiation, (c) thermal radiation, and (d) net radiation.
Figure 5. Net heating at surface of Arctic Ocean.
Figure 6. Seasonal cloud cover for Arctic Ocean for control and GHG experiment. Observations based on Huschke (1969).
Figure 7. Seasonal sea-ice cover for control and GHG simulations and AMIP (see Fig. 2).
Figure 8. Monthly absorbed solar radiation over Arctic Ocean for control (solid line) and GHG experiment (dashed line) at TOA, in the atmosphere, and at the surface. Observed TOA radiation from ERBE (dash-dot line).
Figure 9. Monthly thermal radiation emitted over Arctic Ocean for control (solid line) and GHG experiment (dashed line) at TOA, by atmosphere, and net from surface. Observed TOA emission from ERBE (dash-dot line).
Figure 10. Seasonal net heating at surface of Arctic Ocean.
Figure 11. Ocean liquid heat transport into Arctic Ocean for control and GHG experiment.
Figure 12. Surface air temperature for control and GHG experiment. Observations based on Shea (1986).

Table Captions.

Table 1. Arctic Ocean parameters. Cloud optical depth is a linear average of cloudy and clear-sky conditions.

Table 2. Energy budget of Arctic Ocean (W m^{-2}). Vertical fluxes are positive downward; horizontal fluxes are positive inward.

Table 3. Energy budget of Arctic Ocean for January (W m^{-2}).

Table 4. Energy budget of Arctic Ocean for July (W m^{-2}).

Table 1. Arctic Ocean Parameters. Cloud optical depth is a linear average of cloudy and clear-sky conditions.

	Control	GHG Experiment minus Control		
	1950-2099	1950-99	2000-49	2050-99
Low Cloud Cover (%)	44.325	0.736	1.571	4.900
Totl.Cloud Cover (%)	61.944	1.126	2.685	7.215
Cloud Optical Depth	6.960	0.233	0.559	1.240
Temp.(C) at 200 mb	-59.892	-0.015	-0.159	-0.021
Temp.(C) at 500 mb	-35.629	0.270	0.838	1.760
Temp.(C) at 850 mb	-14.277	0.397	0.989	2.288
Surf.Air Temp.(C)	-13.082	0.576	1.420	3.411
Ground Temp.(C)	-12.827	0.614	1.488	3.688
Ocean Surf.Temp.(C)	-1.319	0.061	0.127	0.376
Sea Ice Mass (kg/m^2	1834.730	-73.070	-185.050	-422.580
Ocean Ice Cover (%)	86.541	-1.648	-3.908	-10.810

Table 2. Energy Budget of Arctic Ocean (W/m^2). Vertical fluxes are positive downward; horizontal transports are positive inward.

	Control	GHG Experiment minus Control		
	1950-2099	1950-99	2000-49	2050-99
Radiation (TOA)	---------	-------	-------	-------
Absorbed Solar	79.71	0.43	1.43	3.17
Net Thermal	-192.64	-0.19	0.01	-1.44
Net Radiation	-112.94	0.24	1.44	1.73
Radiation (Atmos.)				
Absorbed Solar	37.12	0.06	0.22	0.42
Net Thermal	-163.69	-0.62	-1.08	-3.66
Net Radiation	-126.57	-0.56	-0.86	-3.25
Atmos.Heat Transport				
Dry	90.26	-0.59	-1.05	-3.33
Latent	12.33	0.30	0.73	0.83
Total	102.59	-0.29	-0.32	-2.51
Radiation (Surface)				
Incident Solar	92.71	-0.74	-1.87	-4.63
Absorbed Solar	42.59	0.37	1.21	2.76
Downwd.Thermal	231.49	2.90	7.09	17.30
Upward Thermal	-260.45	-2.47	-6.00	-15.08
Net Thermal	-28.96	0.43	1.09	2.22
Surface Fluxes				
Net Radiation	13.63	0.80	2.30	4.98
Sensible Heat	-11.51	-0.40	-0.54	-2.90
Latent Heat	-9.79	-0.40	-0.55	-2.61
Precip.Energy	-2.68	-0.05	-0.09	-0.25
Net Heat	-10.35	-0.05	1.12	-0.78
Water Heat Transport				
Rivers	0.07	0.00	0.00	0.00
Sea Ice	1.58	-0.02	-0.06	-0.70
Liquid Ocean	9.15	0.30	-1.31	0.61
Net Energy Change	0.44	0.22	-0.25	-0.88

Table 3. Energy Budget of Arctic Ocean for January (W/m^2).

	Control	GHG Experiment minus Control		
	1950-2099	1950-99	2000-49	2050-99
Radiation (TOA)	---------	-------	-------	-------
Absorbed Solar	0.11	0.00	0.00	0.00
Net Thermal	-169.28	-0.52	-0.50	-3.18
Net Radiation	-169.17	-0.52	-0.50	-3.17
Radiation (Atmos.)				
Absorbed Solar	0.08	0.00	0.00	0.00
Net Thermal	-129.92	-1.17	-1.03	-6.42
Net Radiation	-129.84	-1.17	-1.02	-6.42
Atmos.Heat Transport				
Dry	105.92	-1.09	-1.86	-7.73
Latent	7.46	0.59	-0.06	-0.08
Total	113.38	-0.51	-1.92	-7.81
Radiation (Surface)				
Incident Solar	0.10	0.00	0.00	-0.01
Absorbed Solar	0.03	0.00	0.00	0.00
Downwd.Thermal	171.91	3.63	7.47	23.76
Upward Thermal	-211.27	-2.98	-6.95	-20.51
Net Thermal	-39.36	0.64	0.52	3.24
Surface Fluxes				
Net Radiation	-39.33	0.64	0.52	3.25
Sensible Heat	-9.40	-0.89	-1.91	-8.40
Latent Heat	-5.35	-0.63	-0.91	-5.16
Precip.Energy	-1.71	-0.16	-0.11	-0.67
Net Heat	-55.79	-1.03	-2.42	-10.99
Water Heat Transport				
Rivers	-0.01	0.00	0.00	0.00
Sea Ice	2.14	0.17	0.28	-0.50
Liquid Ocean	9.00	0.60	-1.34	0.53
Net Energy Change	-44.66	-0.27	-3.48	-10.96

Table 4. Energy Budget of Arctic Ocean for July (W/m^2).

	Control	GHG Experiment minus Control		
	1950-2099	1950-99	2000-49	2050-99
Radiation (TOA)	---------	-------	-------	-------
Absorbed Solar	220.49	0.50	3.19	8.64
Net Thermal	-221.10	0.55	0.90	0.97
Net Radiation	-0.61	1.05	4.09	9.61
Radiation (Atmos.)				
Absorbed Solar	93.23	0.18	0.51	0.73
Net Thermal	-204.99	0.06	0.03	0.09
Net Radiation	-111.77	0.24	0.54	0.81
Atmos.Heat Transport				
Dry	74.90	0.45	1.95	3.81
Latent	21.26	0.90	1.28	1.01
Total	96.16	1.35	3.24	4.81
Radiation (Surface)				
Incident Solar	211.82	-2.18	-2.11	-3.96
Absorbed Solar	127.26	0.32	2.68	7.92
Downwd.Thermal	299.59	0.92	1.51	3.03
Upward Thermal	-315.69	-0.43	-0.64	-2.15
Net Thermal	-16.11	0.49	0.87	0.88
Surface Fluxes				
Net Radiation	111.15	0.81	3.55	8.80
Sensible Heat	-4.39	0.81	1.59	2.36
Latent Heat	-8.18	0.69	1.97	2.65
Precip.Energy	-3.04	0.10	0.22	0.62
Net Heat	95.54	2.40	7.33	14.43
Water Heat Transport				
Rivers	0.14	0.00	0.01	0.02
Sea Ice	0.66	0.03	0.01	-0.49
Liquid Ocean	9.10	0.21	-1.12	0.89
Net Energy Change	105.44	2.64	6.23	14.84

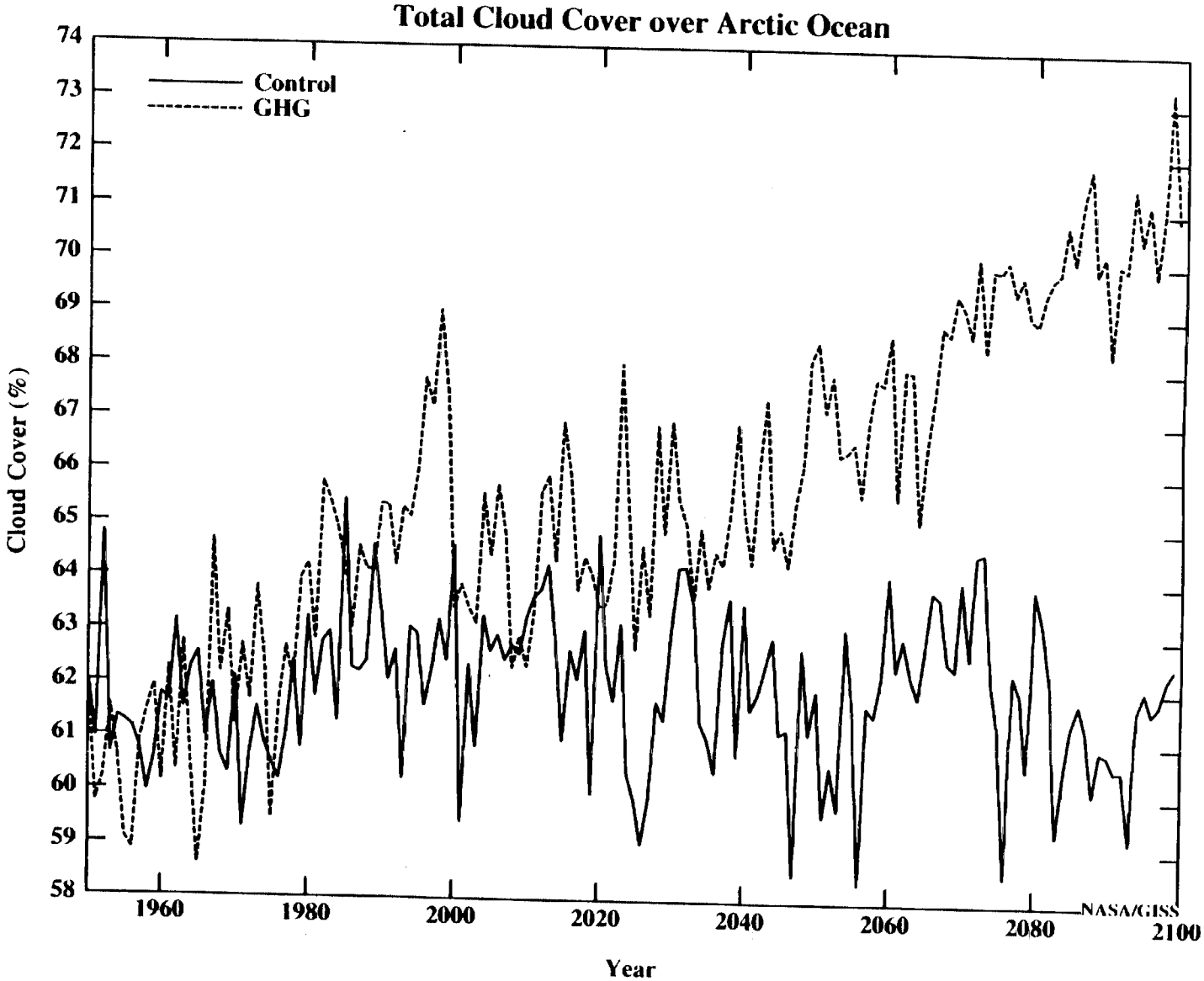

Figure 1. Mean annual cloud cover for Arctic Ocean for control and GHG experiment.

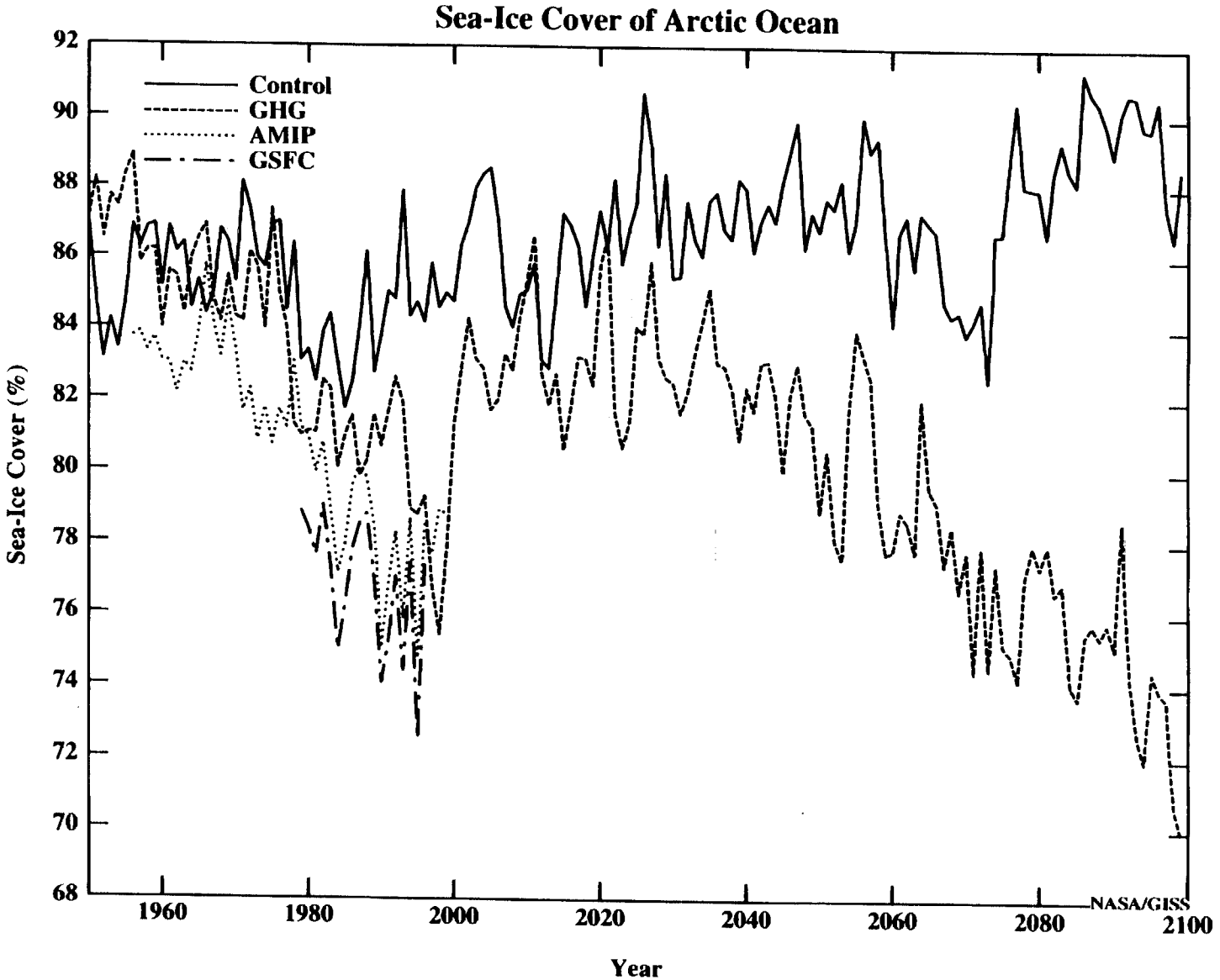

Figure 2. Sea-ice cover for control and GHG experiment. For the observations GSFC (Goddard Space Flight Center) is from Cavalieri et al. (1997) and the AMIP values can be downloaded from http://www-pcmdi.llnl.gov/amip2/AMIP2EXPDSN/BCS/amipobs_dwnld.html.

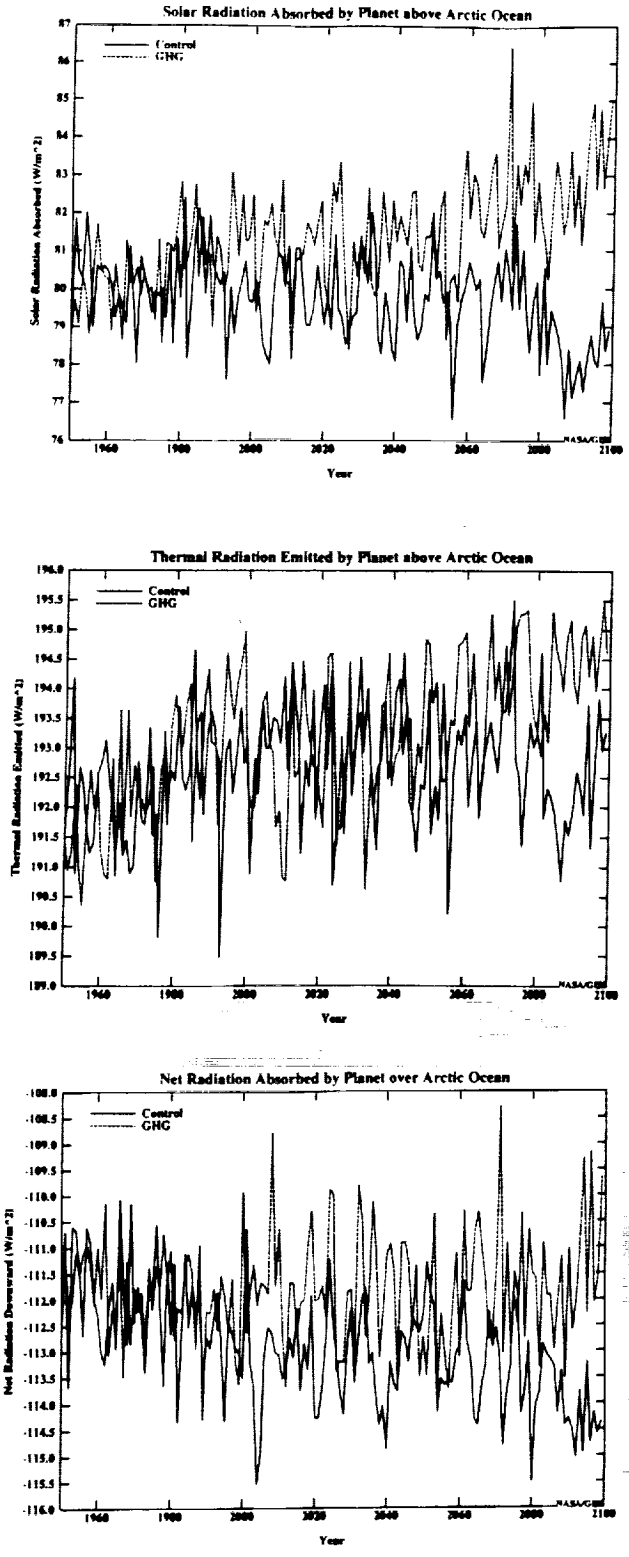

Figure 3. Top of the atmosphere radiation budget for Arctic Ocean for control and GHG experiment for (a) absorbed solar, (b) outgoing thermal, and (c) net downward radiation.

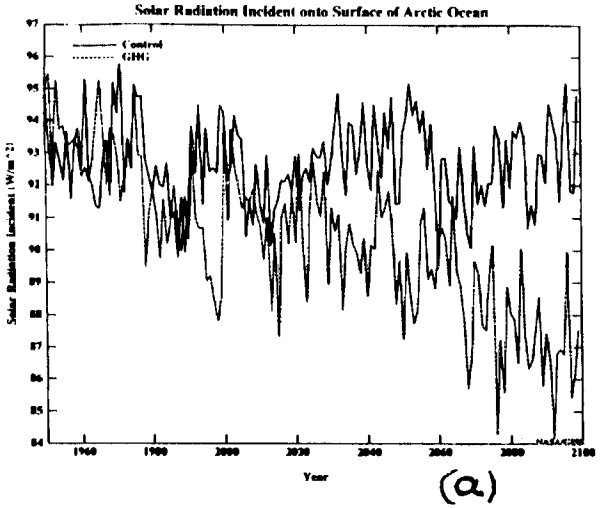

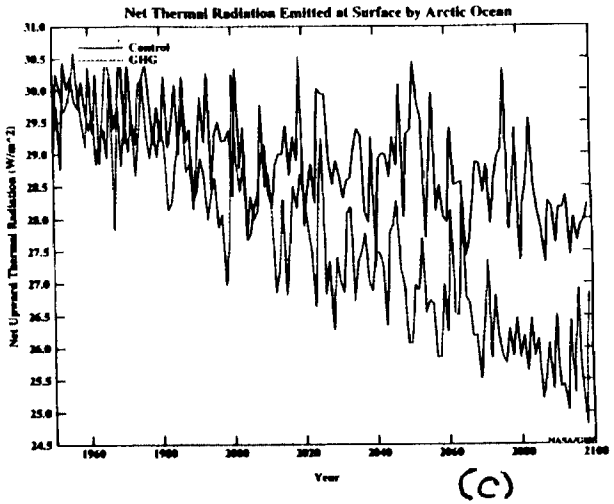

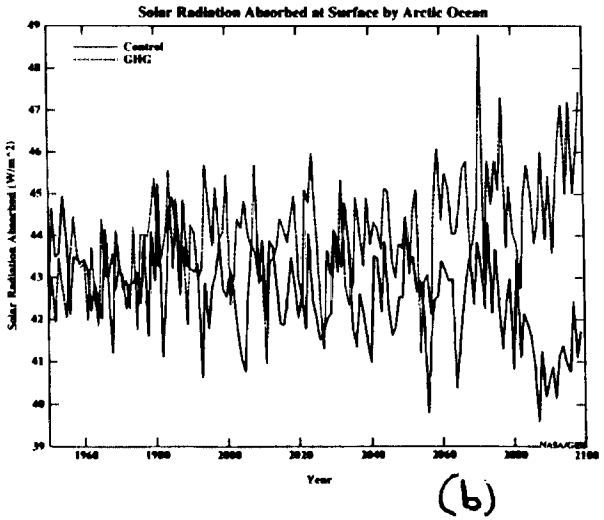

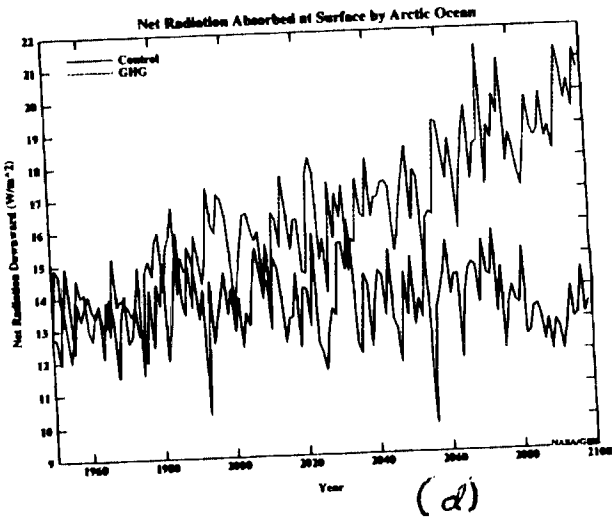

Figure 4. Modeled downward radiation at surface of Arctic Ocean for control and GHG experiment for (a) incident solar radiation, (b) absorbed solar radiation, (c) thermal radiation, and (d) net radiation.

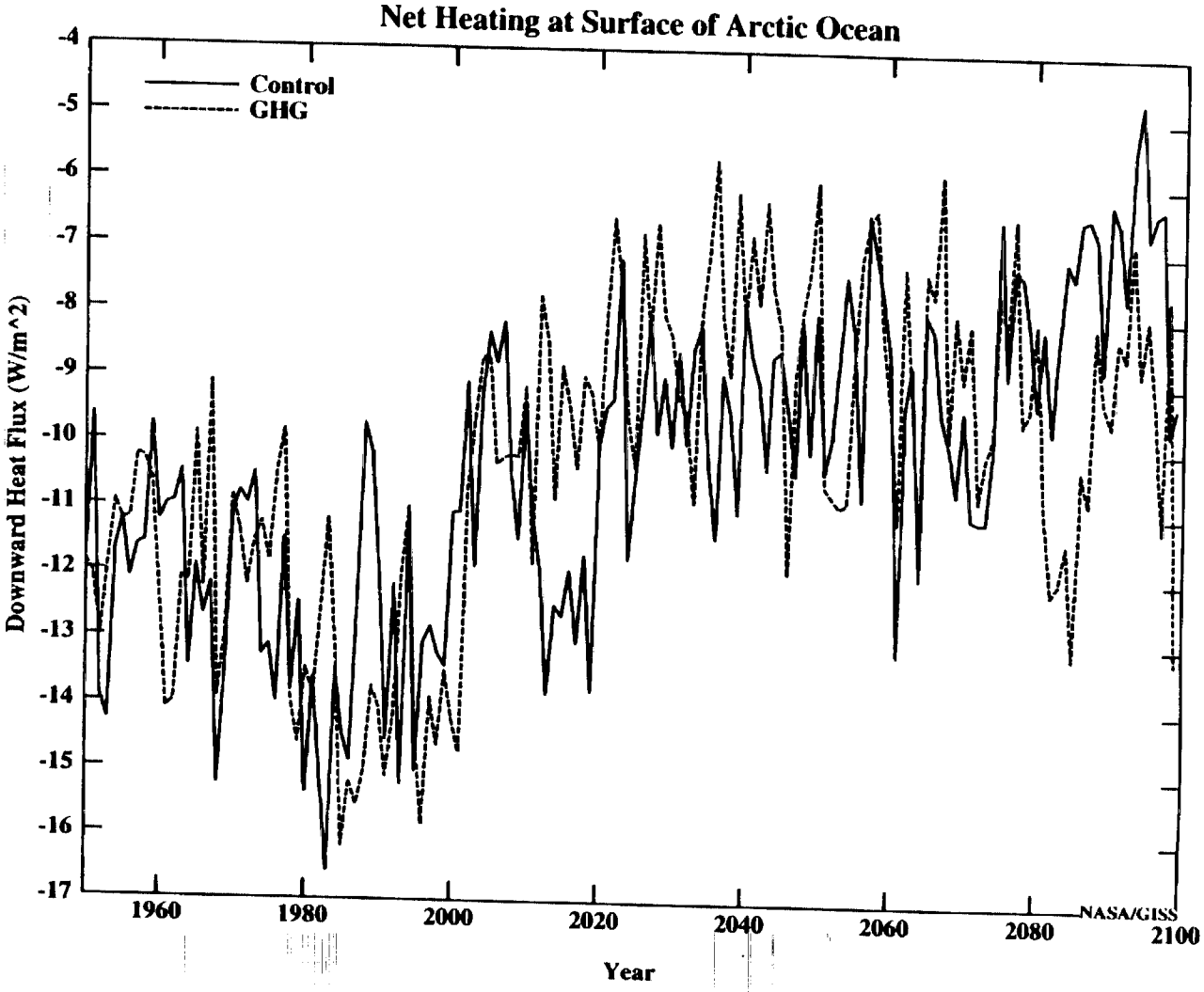

Figure 5. Net heating at surface of Arctic Ocean.

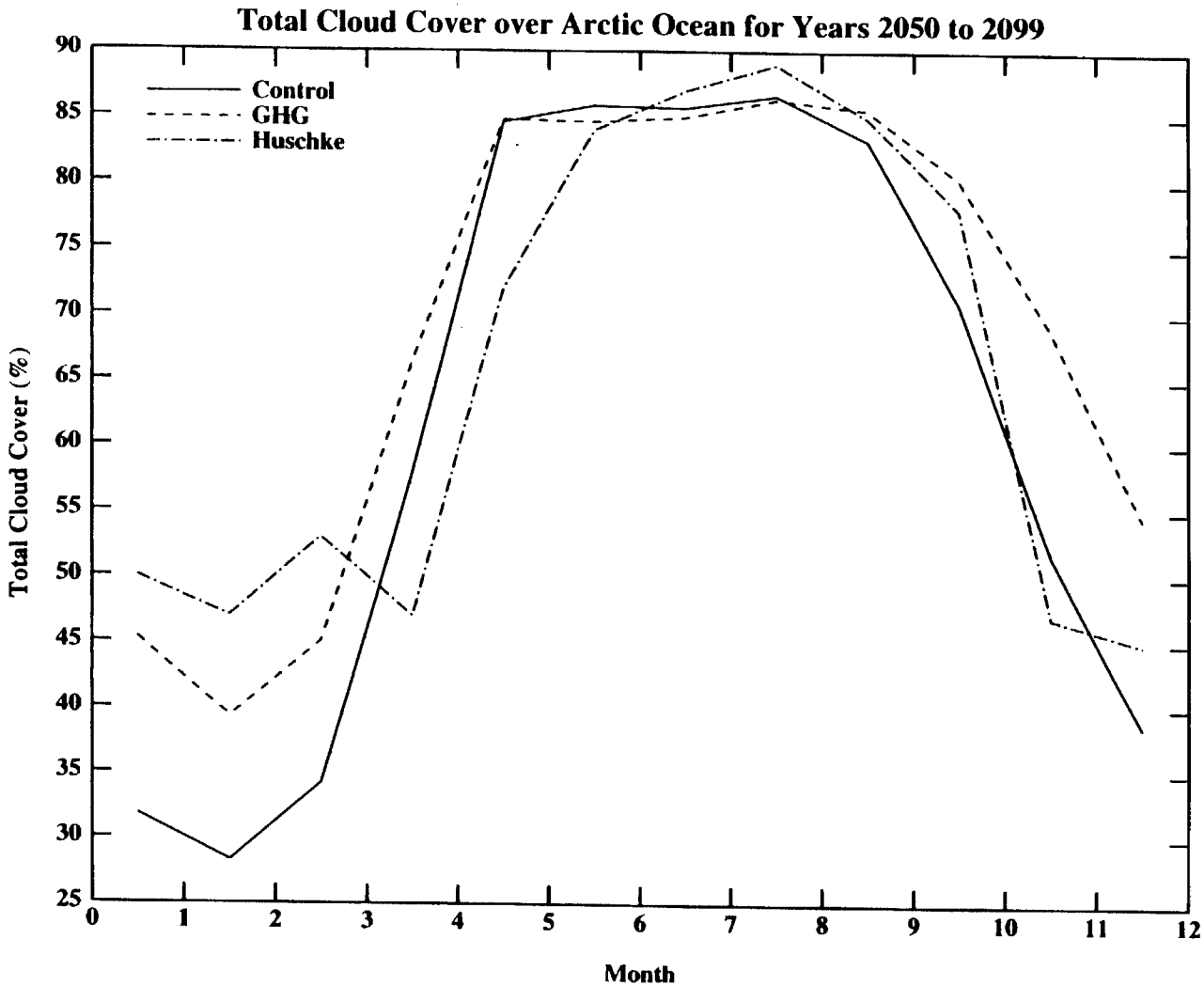

Figure 6. Seasonal cloud cover for Arctic Ocean for control and GHG experiment. Observations based on Huschke (1969).

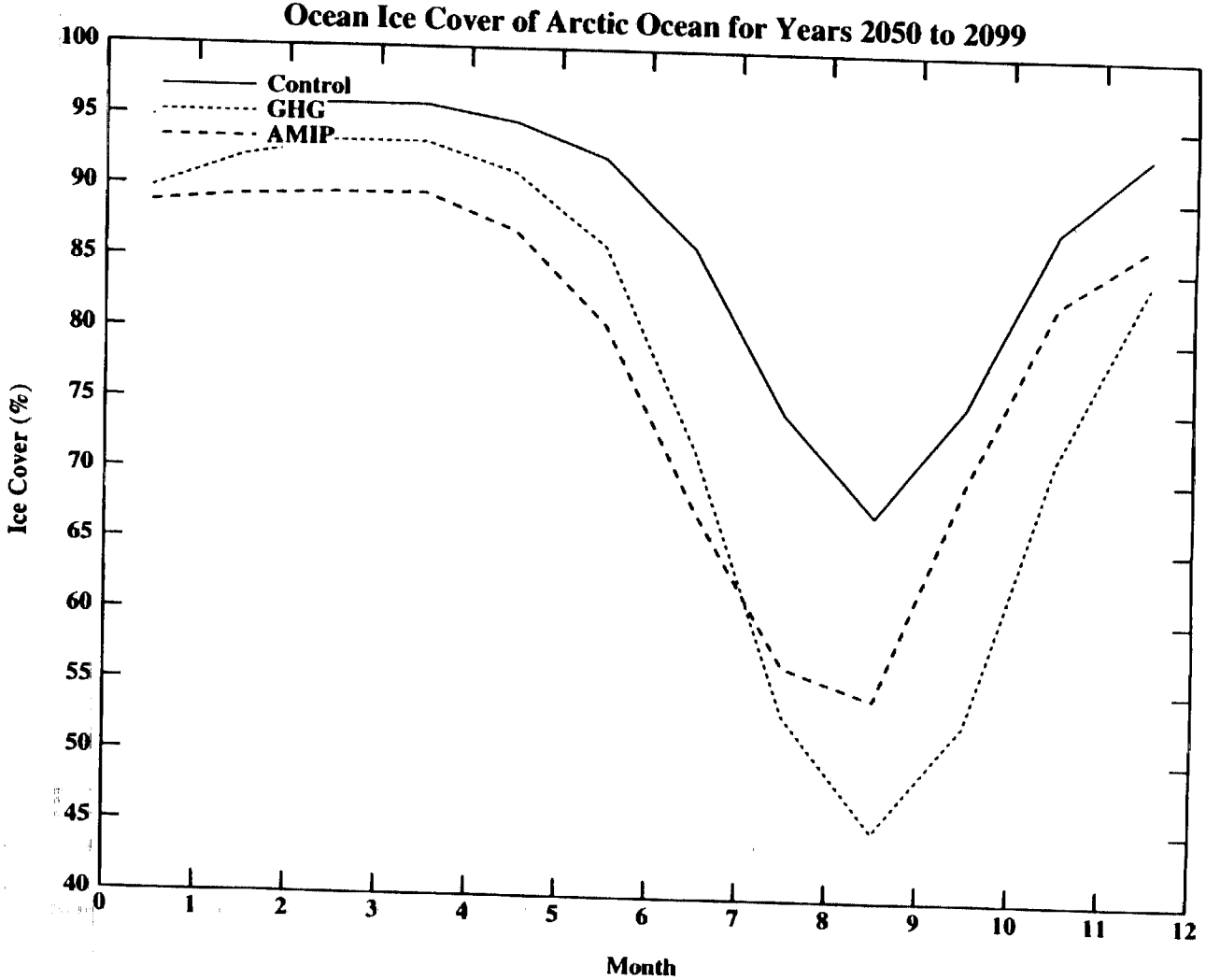

Figure 7. Seasonal sea-ice cover for control and GHG simulations and AMIP (see Fig. 2).

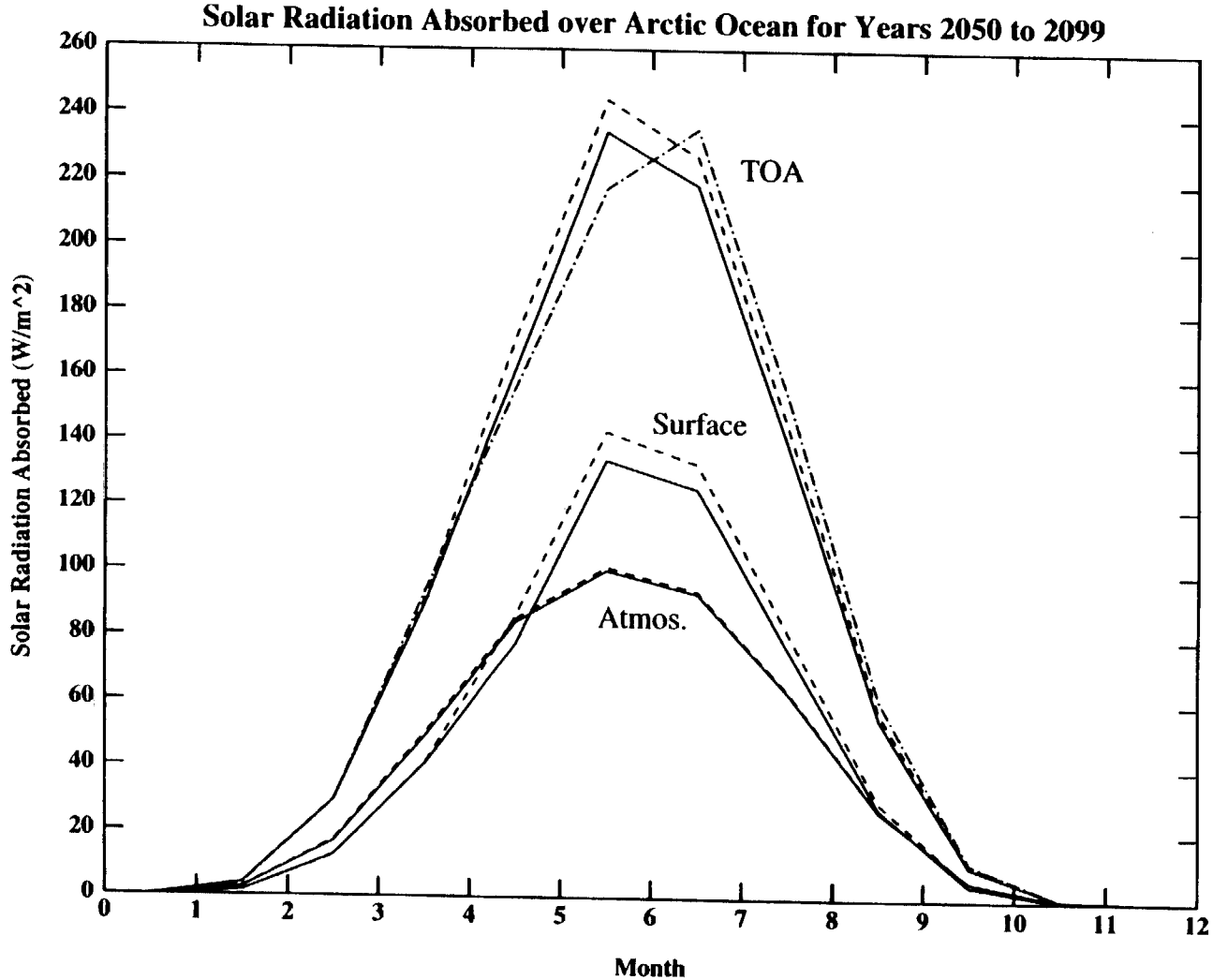

Figure 8. Monthly absorbed solar radiation over Arctic Ocean for control (solid line) and GHG experiment (dashed line) at TOA, in the atmosphere, and at the surface. Observed TOA radiation from ERBE (dash-dot line).

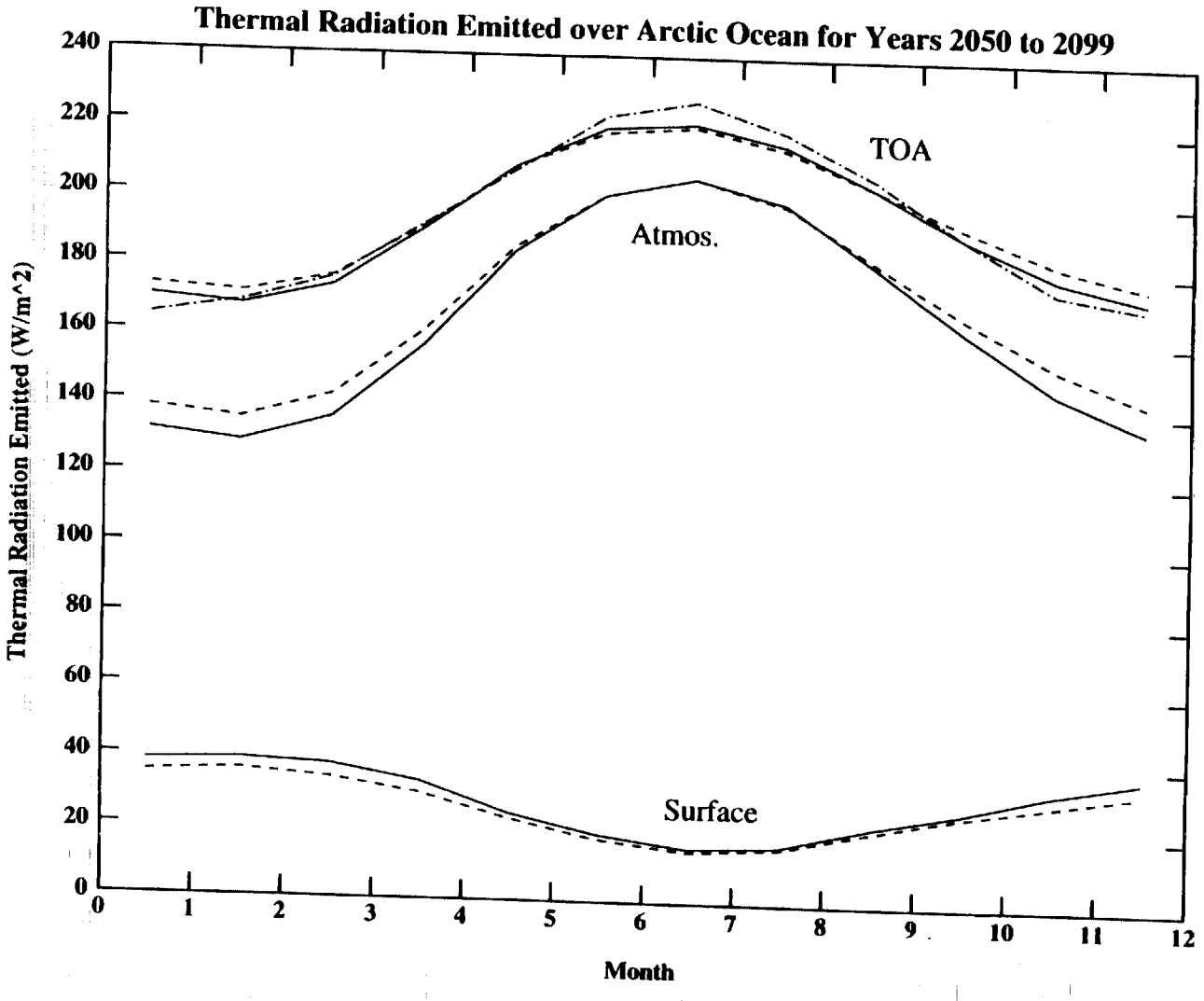

Figure 9. Monthly thermal radiation emitted over Arctic Ocean for control (solid line) and GHG experiment (dashed line) at TOA, by atmosphere, and net from surface. Observed TOA emission from ERBE (dash-dot line).

Fig 11

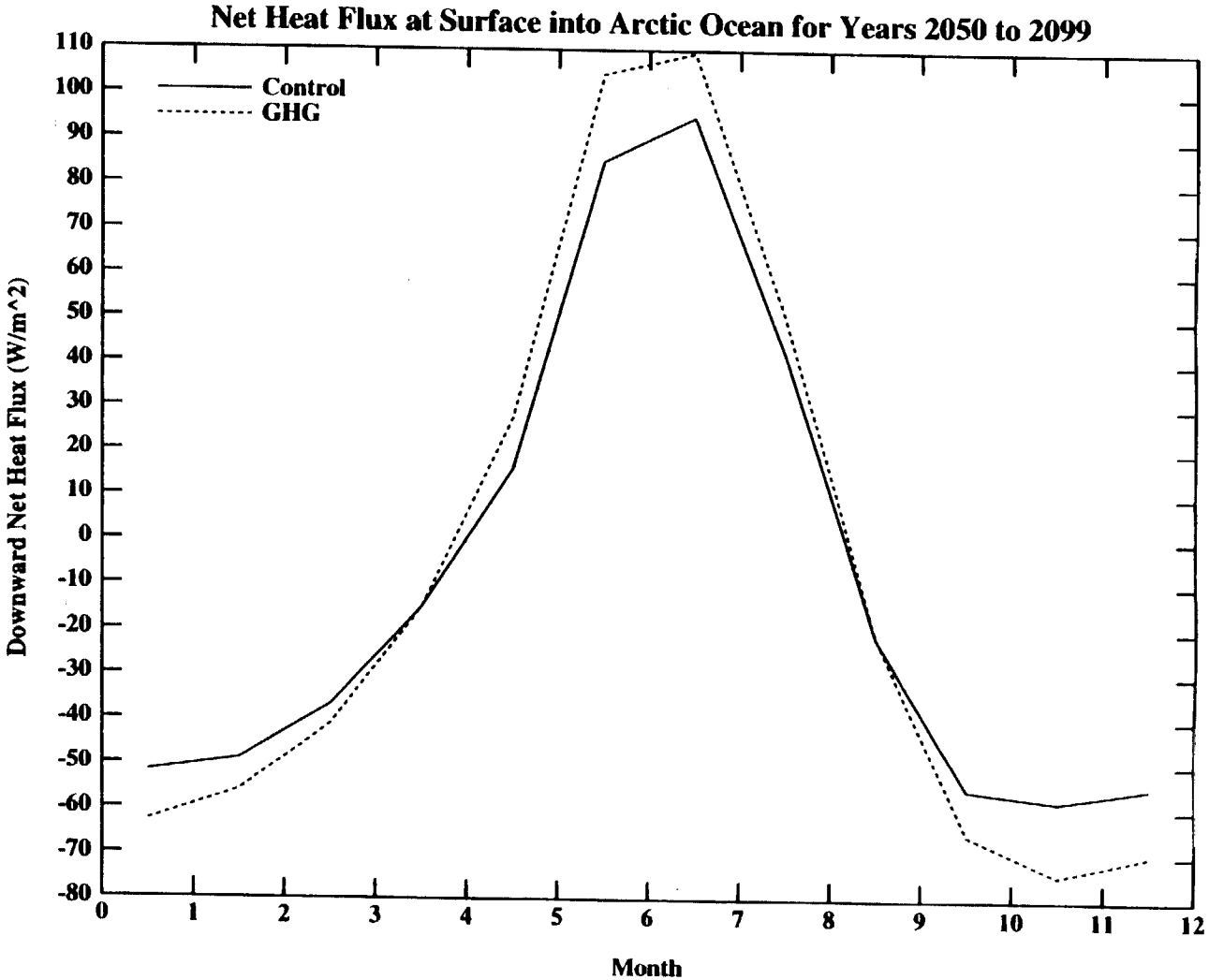

Figure 10. Seasonal net heating at surface of Arctic Ocean.

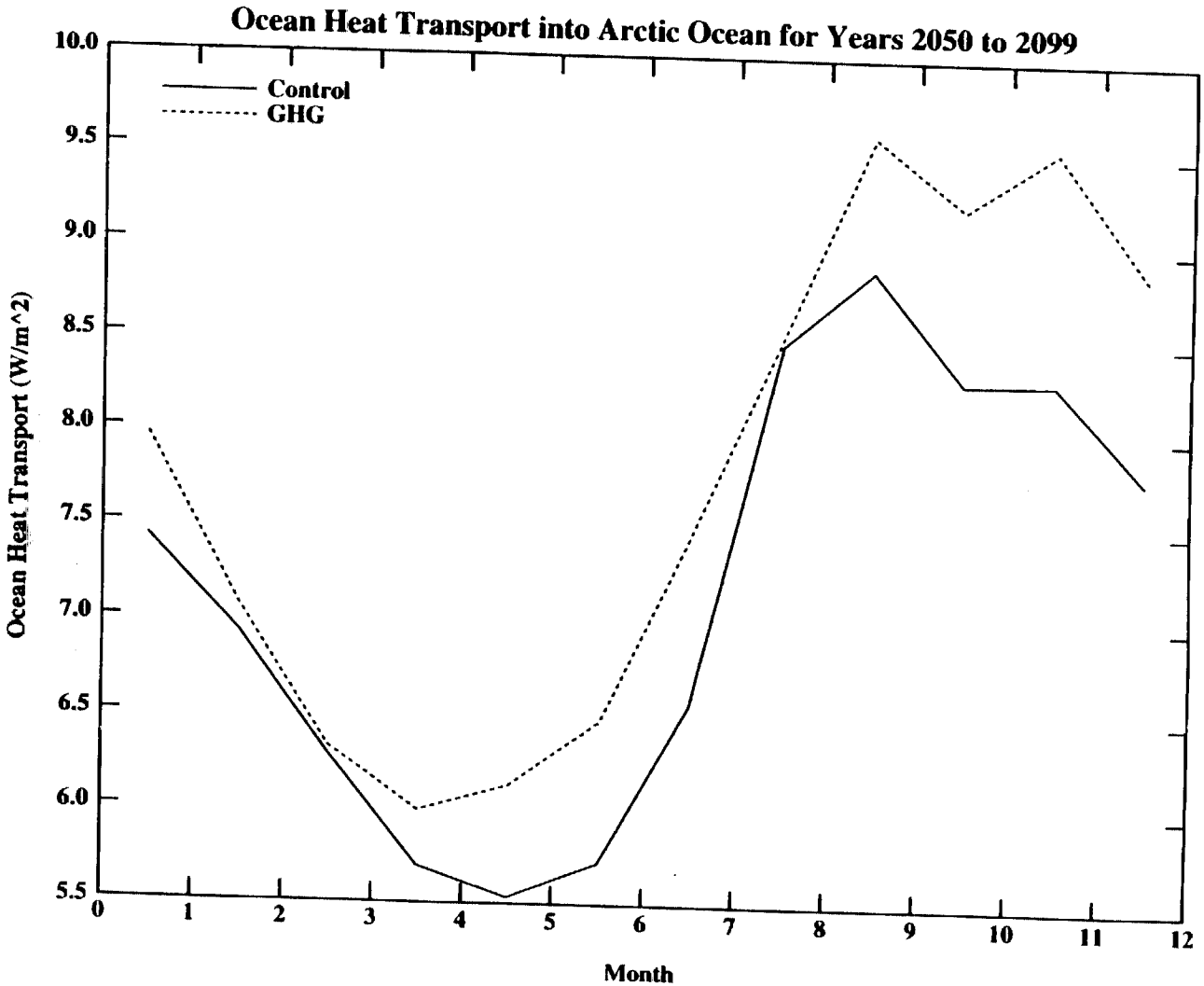

Figure 11. Ocean liquid heat transport into Arctic Ocean for control and GHG experiment.

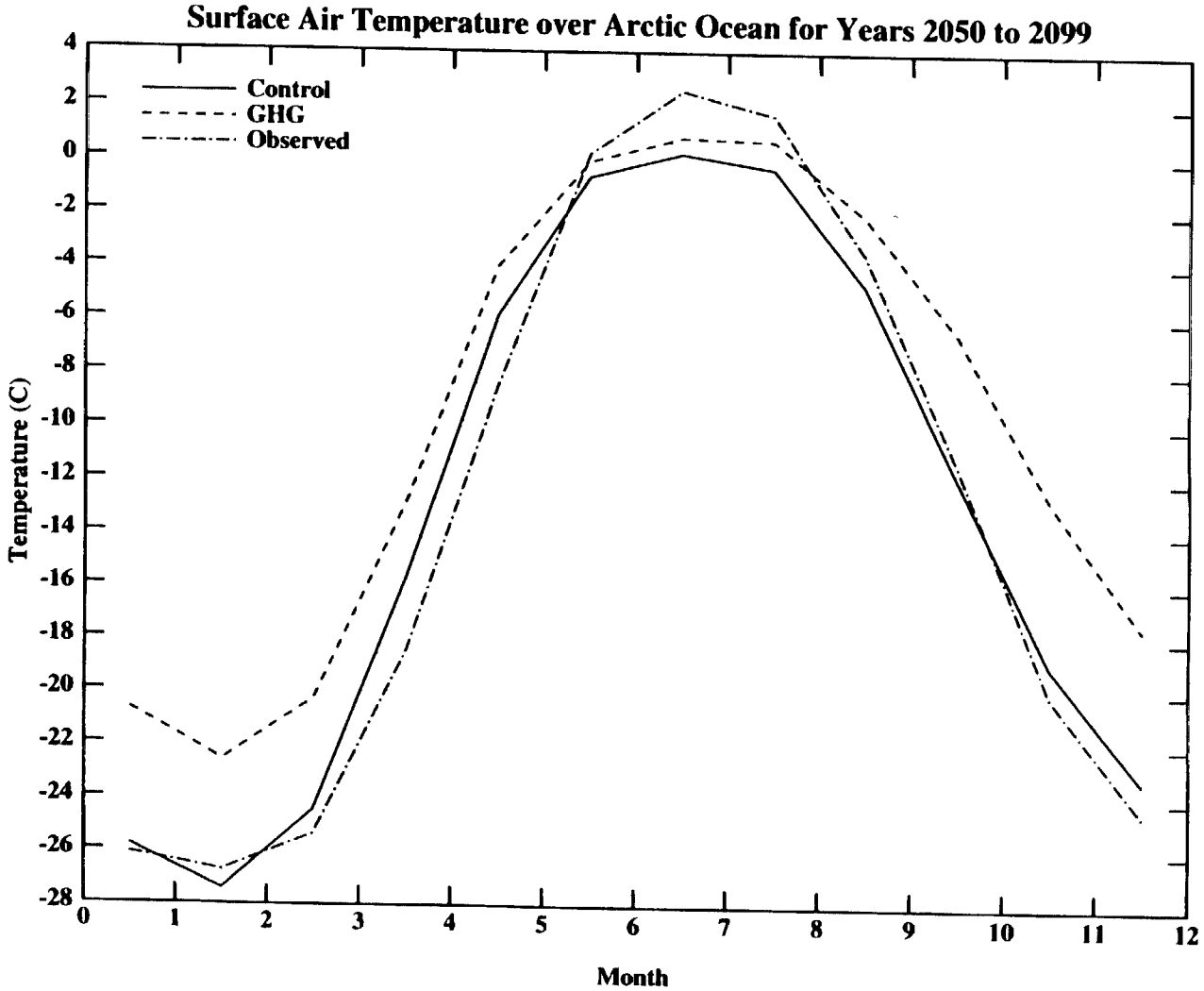

Figure 12. Surface air temperature for control and GHG experiment. Observations based on Shea (1986).